A Simple Multi-Step Solution for Model Predictive Control in Multiphase Electric Drives

I. Gonzalez-Prieto, M.J. Duran, A. Gonzalez-Prieto and J.J. Aciego

***Abstract*– The multiphase electric drive field of research is rather young, and most of the efforts in this area have been focused on appropriately extending different techniques that were already popular in three-phase systems. This is the case of finite-control set model predictive control (FCS-MPC), which has been a hot topic since 2009. Despite the numerous contributions on FCS-MPC for multiphase systems, all of them assume a single-step horizon in the predictions. This paper shows the first attempt to include multistep predictions within the FCS-MPC that performs the current regulation. The extension from the three-phase case is not direct at all because the number of voltage vectors and subspaces is higher, this adding further complexity and eventually leading to issues related to the secondary current regulation. A smart selection of different subsets of voltage vectors is used to ease the implementation, and a modified cost function is developed to jeopardize the high instantaneous voltage values that significantly worsens the current quality at steady state. Experimental results confirm that the use of multistep FCS-MPC is feasible in multiphase electric drives, showing at the same time that some measures must be taken to minimize the distortion in the low-impedance secondary subspaces.**

***Index Terms*– Model predictive control, multiphase electric drives, multistep.**

I. Introduction

Multiphase electric drives is a rather young field of research. Some seminal works from Prof. Thomas Lipo and others were presented in the 90s [1,2], but it was not until the 21st century when Prof. Emil Levi and other researchers further showed the scientific community their potential and exclusive modes of operation [3]. At the same time, the industry also started to consider the multiphase approach as a promising possibility for high current/power applications where reliability becomes the main concern [4], as it is the case of traction applications, wind energy systems or electric vehicles. This interest lasts till the present day, with recent products from emblematic companies such as Mercedes-AMG (EQE 53 4MATIC+ [5]) or Audi (e-tron FE07 [6]) that are using six-phase electric motors on the rear axle to make them particularly powerful [6]. However, the exploitation of all the potential advantages of multiphase electric drives required the development of specific high-performance control techniques [7,8].

In this context, Prof. Federico Barrero et al. started applying model-based predictive control (MPC) to electric machines with more than three phases by 2009 [9], hence funding a growing field of research [10]. The technology of power electronics and digital-signal processors (DSPs) was then sufficiently mature to take up this challenge, and many researchers began to devise different approaches for the real-time implementation of MPC strategies in such multidimensional systems [11].

Initial efforts in FCS-MPC concentrated on the inclusion of restrictions [11,12], the estimation of non-measurable variables [13], the design of fault-tolerant techniques [14-15], the analysis of parameter sensitivity [16], the study of the tradeoffs [17] or the design of new modes of operation [18,19]. More recently, the focus has been shifted to the design of multi-vector strategies in order to further improve the current quality [20-25], proving that FCS-MPC can retain its inherent advantages (e.g., fast transient response or design flexibility) and achieve at the same time a current quality equal or even higher than classical control approaches based on carrier-based pulse-width modulations (PWM) [10]. The control techniques based on multi-vector solutions reduce the harmonic distortion thanks to the suitable application of several switching states during the control period.

Unfortunately, despite the mentioned recent advances in FCS-MPC for multiphase drives, some control alternatives have still not been explored due to the significant demand of computational resources of these special electrical systems. In contrast, in the case of three-phase electric drives, the performance of FCS-MPC has also been enhanced using strategies based on multistep prediction horizons. The use of a higher prediction horizon permits, for instance, a better tracking of the reference variables [26]. In addition, its operating principle is simple and shows a certain relationship with human behavior [26]. For instance, a car driver could enhance his/her performance looking a certain distance in front of his/her car in order to avoid unnecessaries actions and take into account his/her reaction time [26]. In this regard, it is important to highlight that in the field of electric drives due to the usage of a digital control system a one-period control delay appears. Because of the previous implementation limitation, the single-step delay compensation approach is considered as a mandatory action when an FCS-MPC is employed [26]. For this reason, the optimal control action is obtained focusing on the reference variables in $k+2$ although a single-step prediction has been carried out in the control period.

Following with the analysis of the state of art of the multistep FCS-MC solutions, different multistep FCS-MPC proposals have been presented and experimentally validated [27-33]. [29-30] confirmed for a three-phase system the benefits of a long prediction horizon to ensure an adequate closed-loop performance in steady state and to avoid stability limitations. Furthermore, it has been shown that long horizons are potentially beneficial for higher-order

plants, such as converters with an LC filter, where longer horizons can better achieve damping of the resonance [33]. Unfortunately, in spite of the desired benefits of this control alternative, to the best knowledge of the authors, all existing works for multiphase electric drives are based on a single-step prediction horizon [27].

Since the real-time implementation of single-step FCS-MPC already implies a high computational burden, the inclusion of horizons longer than one poses a greater challenge for real-time implementation. Far from being trivial, the extension of multistep FCS-MPC from three to multiphase drives becomes highly challenging. Firstly, the number of switching possibilities is m^n, being m the number of voltage source converter (VSC) levels and n the number of phases, and this implies that the computational burden is highly increased. Consequently, the use of brute force to perform an exhaustive search is essentially impossible when the horizon is higher than one. Secondly, multiphase systems possess a greater number of freedom degrees, and this has significant implications for the multistep design of an FCS-MPC strategy. Apart from standard α-β voltages/currents, regulation techniques must deal with the so-called x-y components when the number of phases is higher than three [8]. In distributed-winding machines with negligible spatial harmonics, these new components do not contribute to the torque production, and consequently, they must be driven to zero for the sake of efficiency [34]. To this end, the switching states of the VSC can be selected in such a manner that the average voltage in the secondary (x-y) plane becomes null [21]. However, it is not the same if the average is null because the voltage is constantly zero or if the average is null because high instantaneous voltages cancel out. In the latter case, even with a zero-average voltage, some switching harmonics would appear [10,35]. In this regard, the creation of a *virtual zero* formed by two active vectors could dramatically worsen the current quality [35] because of the concept of *average deception* detailed in [10]. This is particularly important in multiphase systems because the impedance in the x-y plane is typically very low [34].

In single-step FCS-MPC, this issue has no significance because the control algorithm will just perform the predictions based on a single-prediction horizon. On the contrary, when multistep approaches aim to be implemented, special attention needs to be paid to this issue. In fact, if any action is considered in this regard, the predictive algorithm could be blind to the appearance of current harmonics due to the instantaneous application of active vectors. Because of the usage of several prediction horizons, the algorithm is based on an averaged model, and consequently, it can only *see* average values. However, the promotion of active vectors disregarding the instantaneous values is not advisable since it results in a poor current quality

Based on this insight about the specific problems of multistep FCS-MPC in multiphase systems, this work proposes the first predictive strategy that considers a two-step-horizon predictive control for a six-phase electric drive. The proposal deals with the previously highlighted challenges in the following manner. With regard to the real-time implementation, a subset of 13 voltage vectors from the original $2^6 = 64$ possibilities is selected at time $k + 2$ based on physical considerations. Only large and zero voltage vectors are selected at this stage since they provide the best ratio of α-β to x-y voltage production [36]. Then, another subset is selected at time k+3 that includes the large adjacent voltage vectors in the α-β plane (in relation to the one that has been previously evaluated) plus one vector in phase opposition. The null voltage vector is also added as an available solution for the second prediction horizon ($k + 3$). The number of iterations with this choice is equal to 52, which is admissible for a real-time application with standard DSPs. It is likely that longer horizons would require the application of a branch-and-bound search (or similar), but for this initial proof of concept with multiple steps, physical considerations suffice to achieve an adequate DSP implementation.

Although the restrictions on the number of switching states to be evaluated allow the real-time implementation, it is still necessary to deal with the problems associated to the *average deception* [10]. For this purpose, a new cost function is proposed, including a term related to the standard deviation of secondary currents. With this procedure, the control algorithm also considers the current harmonics due to instantaneous values, leading to a significant reduction of the current harmonic distortion.

To sum up, this paper presents the first implementation of multistep FCS-MPC for a multiphase electric drive with two main novelties: a smart selection of the available voltage vectors and a modified cost function that indirectly considers the instantaneous values. The first novelty is based on the previous knowledge of the physical system, whereas the second one stems from the understanding of the problems associated with the *average deception* concept. Finally, it is important to highlight that the considered multi-step algorithm can also be implemented using different multi-vector solutions in order to increase the system performance. In fact, thanks to the proposed control structure, the set of selectable control actions can be modified in a simple manner.

The paper is structured as follows. Section II describes the generalities of the employed six-phase electric drives. In Section III the proposed multistep FCS-MPC is introduced in a detailed manner. The experimental results are shown in Sections IV, whereas, finally, the main conclusions are summarized in Section V.

II. Six-phase Electric Drives Generalities

The selected electrical drive is formed by an asymmetrical six-phase induction machine (IM) fed by a dual two-level three-phase VSC. The stator windings of the considered IM are distributed and spatially shifted 30°. Moreover, the multiphase machine is configured with two isolated neutral points, simplifying the regulation stage [37]. As shown in Fig. 1, each stator winding set is fed by a two-level VSC. The selected topology provides 64 switching states (2^6) to regulate the multiphase IM.

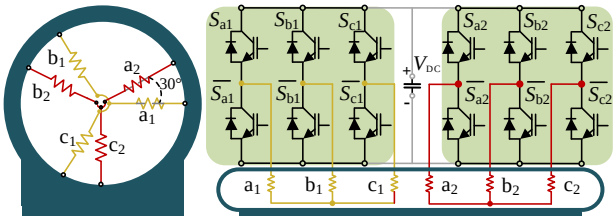

Fig.1. Topology of the selected six-phase electric drive.

It is possible to obtain the stator phase voltages (v_{ij}) from the available VSC switching states (S_{ij}) and the DC-link voltage (V_{DC}) as follows:

$$\begin{bmatrix} v_{a1} \\ v_{b1} \\ v_{c1} \\ v_{a2} \\ v_{b2} \\ v_{c2} \end{bmatrix} = \frac{V_{DC}}{3} \cdot \begin{bmatrix} 2 & -1 & -1 & 0 & 0 & 0 \\ -1 & 2 & -1 & 0 & 0 & 0 \\ -1 & -1 & 2 & 0 & 0 & 0 \\ 0 & 0 & 0 & 2 & -1 & -1 \\ 0 & 0 & 0 & -1 & 2 & -1 \\ 0 & 0 & 0 & -1 & -1 & 2 \end{bmatrix} \cdot \begin{bmatrix} S_{a1} \\ S_{b1} \\ S_{c1} \\ S_{a2} \\ S_{b2} \\ S_{c2} \end{bmatrix}, \quad (1)$$

where $[S_{ij}]$ describes the switching state of the different VSC legs using a binary value. If the upper switch of the leg is ON and the lower switch is OFF $S_{ij} = 1$, and $S_{ij} = 0$ if the opposite occurs.

Focusing on the IM, phase variables describe its performance, but diverse reference frames can be employed to facilitate the understanding and the regulation of the IM. Literature contains different reference frames and transformations for that purpose, being the vector space decomposition (VSD) a widespread option [38]. In this stationary reference frame, phase variables are mapped onto three orthogonal subspaces with a clear physical meaning. In this regard, the amplitude-invariant Clarke transformation is typically applied:

$$[C] = \frac{1}{3} \cdot \begin{bmatrix} 1 & -1/2 & -1/2 & \sqrt{3}/2 & -\sqrt{3}/2 & 0 \\ 0 & \sqrt{3}/2 & -\sqrt{3}/2 & 1/2 & 1/2 & -1 \\ 1 & -1/2 & -1/2 & -\sqrt{3}/2 & \sqrt{3}/2 & 0 \\ 0 & -\sqrt{3}/2 & \sqrt{3}/2 & 1/2 & 1/2 & -1 \\ 1 & 1 & 1 & 0 & 0 & 0 \\ 0 & 0 & 0 & 1 & 1 & 1 \end{bmatrix}, \quad (2)$$

$$[v_{\alpha s}, v_{\beta s}, v_{xs}, v_{ys}, v_{z1}, v_{z2}]^T = [C] \cdot [v_{a1}, v_{b1}, v_{c1}, v_{a2}, v_{b2}, v_{c2}]^T,$$

$$[i_{\alpha s}, i_{\beta s}, i_{xs}, i_{ys}, i_{z1}, i_{z2}]^T = [C] \cdot [i_{a1}, i_{b1}, i_{c1}, i_{a2}, i_{b2}, i_{c2}]^T.$$

The main subspace (α-β) permits the flux/torque production, whereas the x-y plane, is solely related to stator copper losses in distributed-winding machines with negligible spatial harmonics. On the other hand, the zero-sequence currents (z_1– z_2) are null due to the use of two isolated neutral points.

The stator phase voltages can be mapped onto α-β and x-y planes as shown in Fig. 2. Active voltage vectors of the main plane inherently show an active contribution in the secondary subspace. In Fig. 2 each voltage vector is designated using a decimal value equivalent to the binary code of the switching state $[S]$. The available control actions can be sorted depending on their magnitude in the main plane as: large (C_L), medium-large (C_{ML}), medium (C_M), small (C_S) and null voltage vectors.

Furthermore, it is possible to achieve a decoupled flux/torque regulation using the rotating d-q reference frame. In this manner, the torque generation is exclusively related to the q–component, whereas the flux production is subjected to the d–component. This decoupling process is carried out using the Park transformation (3):

$$[D] = \begin{bmatrix} cos\theta & sin\theta \\ -sin\theta & cos\theta \end{bmatrix}, \quad (3)$$

where θ, calculated using the measured speed and the estimated slip [36], represents the angle of the rotor flux.

III. MultiStep Model Predictive Control

A. Multistep MPC structure

The proposed FCS-MPC scheme shows a similar structure as in the case of the classical version of this non-linear regulation strategy. In other words, an outer control loop

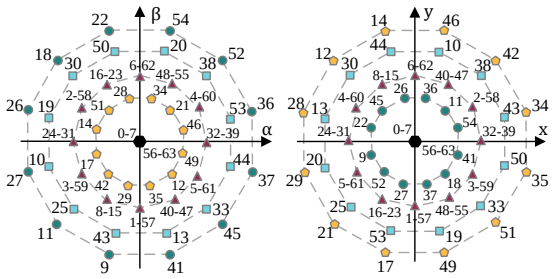

Fig. 2. Map of the voltage vectors in the α-β and x-y subspaces.

ensures the tracking of the reference speed (ω_m^*) using a proportional-integral (PI) controller, whereas the inner control loop uses a predictive machine model to satisfy the current control (see Fig. 3). Focusing on the current regulation (α-β and x-y components), a discretized machine model based on the Euler discretization is implemented in this work:

$$\frac{d}{dt}[X_{\alpha\beta}] = [A] \cdot [X_{\alpha\beta xy}] + [B] \cdot [U_{\alpha\beta xy}], \quad (4)$$

where:

$$[U_{\alpha\beta xy}] = [v_{\alpha s}\ v_{\beta s}\ v_{xs}\ \ v_{ys}\ 0\ 0]^T,$$
$$[X_{\alpha\beta xy}] = [i_{\alpha s}\ i_{\beta s}\ i_{xs}\ i_{ys}\ \lambda_{\alpha r}\ \lambda_{\beta r}]^T, \quad (5)$$

matrices $[A]$ and $[B]$ define the dynamic behavior of machine and they are parameter dependent [13]. On the other hand, $\lambda_{\alpha\beta r}$ expresses the rotor flux production in the main plane.

As in the case of standard FCS-MPC (see flowchart in Fig.4), the one-step delay approach is also implemented in the proposed multistep scheme (Fig. 3). However, since a multistep horizon is employed in this work, the flow diagram of conventional MPC schemes needs to be reformulated. In the designed multistep solution, the predictive model is employed three times per control period. In the standard version of FCS-MPC based on a single-prediction horizon, the predictive model is employed twice per sampling period, as shown in Fig. 4. Focusing on the proposed strategy, the machine model is firstly employed to obtain the phase currents in k+1, and, later, to estimate the predicted currents in k+2 and k+3 (Fig. 5). Finally, the reference ($i^*_{\alpha\beta xys}\big|_{k+3}$) and predicted currents ($\hat{\imath}_{\alpha\beta xys}\big|_{k+3}$) are compared in a predefined cost function to obtain the optimal switching state for the next control period.

The performance of the proposed multistep FCS-MPC strategy highly depends on the smart design of the control action subsets and the development of a new cost function to avoid the *average deception* described in [10]. For that reason, the next subsections describe the foundations of the selected approaches for these two issues.

B. Designing a selective criterion for control actions

A reduced set of switching states needs to be defined as available control actions in order to fulfill the more restrictive scenario from the point of view of the real-time implementation of a multistep FCS-MPC. In this regard, large voltage vectors of Fig. 2 are considered as the active voltage actions of this work. They achieve the maximum flux/torque production with a reduced contribution in the secondary plane. Moreover, the zero-switching state is also considered as a selectable control action. In this way, a total of 13 voltage vectors are evaluated in k+2 for the proposed FCS-MPC. This approach implies a significant reduction in the number of switching states in comparison with the original case. However, the real-time implementation of the proposed

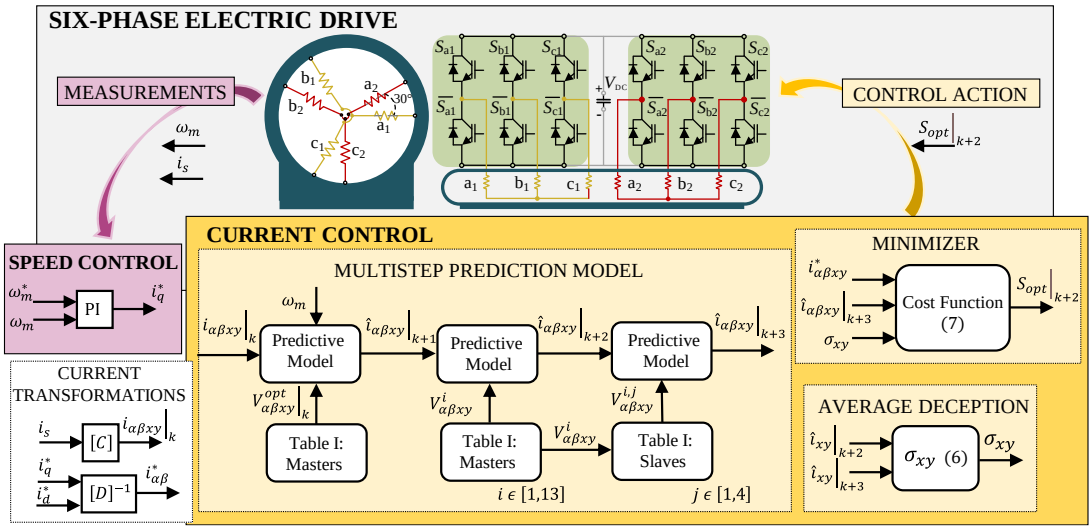

Fig. 3. Scheme of the proposed multistep horizon FCS-MPC.

control scheme requires an extra decrease in the number of possible combinations for the second prediction step.

For that purpose, different subsets of voltage vectors have been created to be employed in the second prediction step (k+3). In fact, 12 different subsets of control actions were designed offline. Each set is characterized by a master voltage vector ($V^{i}_{\alpha\beta xy}$) for k+2, and they also include the four possible voltage combinations for k+3, slave vectors ($V^{i,j}_{\alpha\beta xy}$) (see Table I). Thus in k+3, each large voltage vector can only be combined with three active control actions and the zero state. This approach permits a significant reduction of the necessary voltage evaluations, in fact, only 52 iterations are carried out.

In order to simplify the comprehension of the construction criterium employed in the design of the proposed subsets, the voltage vector V_{37} is considered as an example (without lack of generality thanks to symmetry considerations). Focusing on its adjacent voltage vectors V_{36} and V_{45}, this multistep switching pattern permits at the same time a suitable flux/torque production and a low harmonic distortion thanks to their suitable location in both subspaces. Specifically, adjacent vectors are close in the α-β plane and almost in opposite phase in the x-y plane (150º apart), hence generating large voltages in the primary subspace and a high cancellation in the secondary subspace. Furthermore, adjacent vectors have another beneficial property: the number of VSC switch changes is only one, leading to a low effective switching frequency. Apart from the features related to the location and the switching pattern, it is worth highlighting that in steady-state operation, it is well-known that the voltage describes a circle in the α-β plane. Therefore, the generation of a rotating α-β voltage vector requires moving to adjacent voltages. Consequently, the selection of adjacent voltage vectors for k+3 is appropriate to cancel x-y components, to minimize the switching frequency and to create a rotating flux. On the other hand, the voltage vector in the opposite phase with V_{37} is also added to its corresponding subset, providing the ability to satisfy sudden voltage output changes. Finally, the zero-switching state is considered as a selectable voltage option for the k+3 horizon. This combination allows a null-voltage contribution in the second prediction horizon and, consequently, a reduced harmonic content can be achieved in this last prediction horizon.

Focusing on the usage of the proposed multi-step algorithm when several switching states are applied per sampling period, the control designer only needs to modify the Table I according to the selected multi-vector solution.

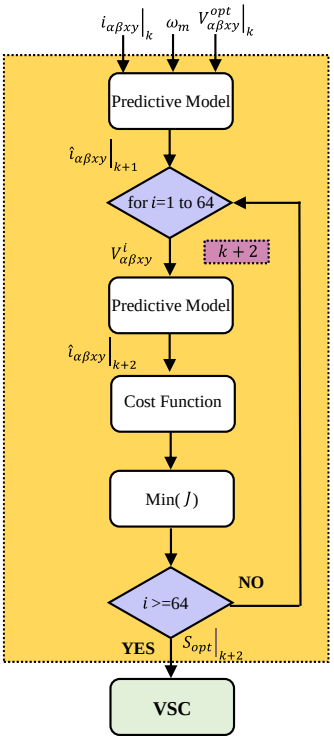

Fig. 4. Flowchart of standard FCS-MPC.

TABLE I.
MULTISTEP CONTROL ACTIONS FOR K+2 AND K+3

Master k+2	Slave #1 k+3	Slave #2 k+3	Slave #3 k+3	Slave #4 k+3
V_{37}	V_{45}	V_{36}	V_{26}	V_0
V_{36}	V_{37}	V_{52}	V_{27}	V_0
V_{52}	V_{36}	V_{54}	V_{11}	V_0
V_{54}	V_{52}	V_{22}	V_9	V_0
V_{22}	V_{54}	V_{18}	V_{41}	V_0
V_{18}	V_{22}	V_{26}	V_{45}	V_0
V_{26}	V_{18}	V_{27}	V_{37}	V_0
V_{27}	V_{26}	V_{11}	V_{36}	V_0
V_{11}	V_{27}	V_9	V_{52}	V_0
V_9	V_{11}	V_{41}	V_{54}	V_0
V_{41}	V_9	V_{45}	V_{22}	V_0
V_{45}	V_{41}	V_{37}	V_{18}	V_0
V_0	V_0	V_0	V_0	V_0

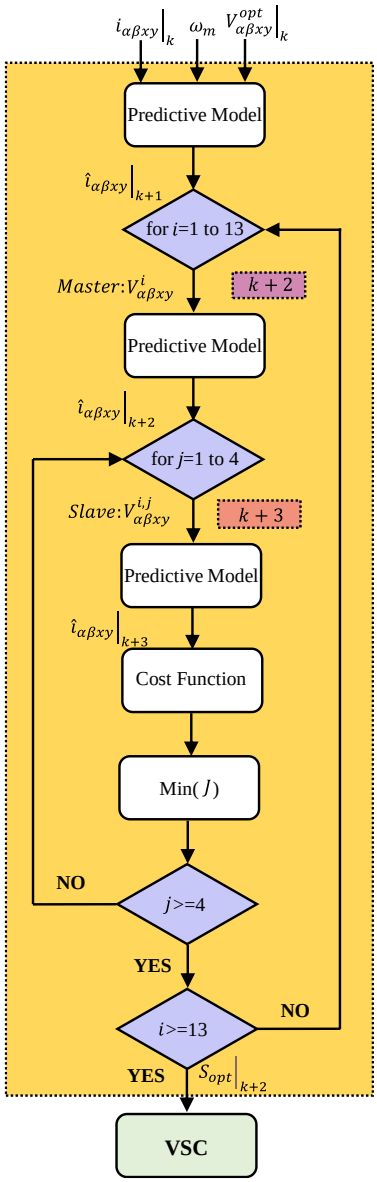

Fig. 5. Flowchart of the proposed multistep FCS-MPC.

C. Avoiding the average deception

The proposed cost function has been designed to achieve a suitable tracking of the flux/torque requirements and a mitigated harmonic distortion, although a single switching state is applied per sampling period. The use of a double prediction horizon can limit the capability of the control scheme to achieve a suitable current quality if the instantaneous values are neglected. Concerning the regulation of the secondary subspace, the ideal voltage selection is to obtain a null-average production with minimal current injection. This second requirement is crucial to avoid that the optimal voltage vector selection can be based on the creation of a *virtual zero* voltage. This control constraint is addressed in this work with the development of a term related to the standard deviation of the x-y currents in the multistep prediction horizon:

$$\sigma_x = \frac{1}{2}\cdot(\hat{\imath}_{xs}|^2_{k+2} + \hat{\imath}_{xs}|^2_{k+3}) - (\hat{\imath}_{xs}|_{k+2}\cdot\hat{\imath}_{xs}|_{k+3}),$$
$$\sigma_y = \frac{1}{2}\cdot\left(\hat{\imath}_{ys}\big|^2_{k+2} + \hat{\imath}_{ys}\big|^2_{k+3}\right) - \left(\hat{\imath}_{ys}\big|_{k+2}\cdot\hat{\imath}_{ys}\big|_{k+3}\right). \quad (6)$$

Searching for the reduction of the instantaneous current injection in the secondary subspace and consequently a suitable current quality, the term (6) is added to the proposed cost function

$$J = e^2_{\alpha s} + e_{\beta s}{}^2 + K_{xy}\cdot(e_{xs}{}^2 + e_{ys}{}^2) + K_{sd}\cdot(\sigma_x + \sigma_y), \quad (7)$$

where:

$$e_{\alpha s} = i^*_{\alpha s} - \hat{\imath}_{\alpha s}|_{k+3},$$
$$e_{\beta s} = i^*_{\beta s} - \hat{\imath}_{\beta s}\big|_{k+3},$$
$$e_{xs} = i^*_{xs} - \hat{\imath}_{xs}|_{k+3}, \quad (8)$$
$$e_{ys} = i^*_{ys} - \hat{\imath}_{ys}\big|_{k+3},$$

being K_{xy} and K_{sd} the weighting factors defined to prioritize the different control objectives.

In summary, the new added term promotes voltage profiles with no sudden changes within $k+2$ (for the same average value) and, conversely, jeopardizes those voltage vectors that have a shape profile and generate high current harmonics.

IV. Experimental Results

A. Test Bench

Experimental testing has been carried out using the test bench shown in Fig. 6. The six-phase drive employed to validate this work is formed by an asymmetrical six-phase IM fed by a dual two-level three-phase VSC (Semikron SKS22F modules). A single DC-link feeds this VSC topology. The IM drive parameters have been obtained using AC time domain and stand-still with inverter supply tests [39-40]. These parameters and rated values are included in Table II.

A single DC power supplies the VSCs, and the control actions are performed by a digital signal processor (TMS320F2833 from Texas Instruments, TI) programmed using a J-TAG and the TI proprietary software named Code Composer Studio. Four Hall-effect sensors (LEM LAH 25-NP) and a digital encoder (GHM510296R/2500) are employed to acquire current and speed data, respectively. The six-phase IM is loaded coupling its shaft to a DC machine acting as a generator. The armature of this DC machine is connected to a variable passive load which allows power to be dissipated, and the load torque is consequently speed dependent.

B. Experimental results

The goodness of the proposed multistep FCS-MPC, where the control focus is established in $k+3$, is firstly evaluated at high speed (800 rpm) in steady-state condition (Test 1). Apart from the standard use of a weighting factor to find a trade-off between main and secondary planes (i.e., K_{xy}), the current proposal includes a new term (K_{sd}) that considers the variability of the control actions within the two considered sampling periods. Aiming to highlight the importance of both terms, Test 1 will include the results at the same operating point, but with different settings of the weighting factors:

Test 1.1: with a null value of K_{sd} to evaluate the performance with just average considerations (see left plots in Fig. 7).

Test 1.2: with a null value of K_{xy} to test the performance when only instantaneous values are taken into account (see middle plots in Fig. 7)

Test 1.3: with non-null values of both K_{xy} and K_{sd} to assess the performance when both average and instantaneous values are considered (see right plots in Fig. 7).

When only average values are considered (Test 1.1), it can be observed that both the speed and currents are correctly tracked (Fig. 7a and 7b). The currents of the secondary plane

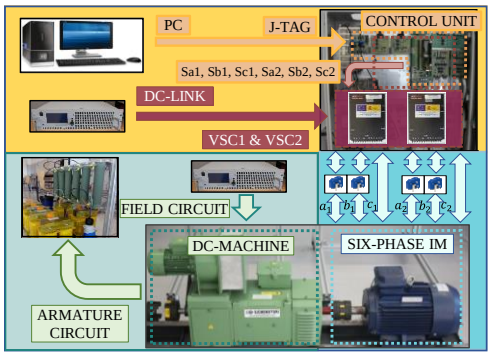

Fig. 6. Scheme of the test bench used for the experimental results.

TABLE II
SIX-PHASE IM DRIVE AND CONTROL PARAMETERS

Parameter		Value
P_{rated}(kW)	Power	1
V_{DC}(V)	DC-link voltage	300
$T_{rated}(N \cdot m)$	Rated torque	10
I_{peak}(A)	Peak current	4.5
ω_{rated}(r/min)	Rated speed	1000
R_s (Ω)	Stator resistance	4.20
R_r (Ω)	Rotor resistance	3
L_m(mH)	Mutual inductance	280
L_{ls}(mH)	Stator leakage inductance	4.5
L_{lr}(mH)	Rotor leakage inductance	55.12
T_s(μs)	Control/Sampling period	100

are also forced to be around zero (Fig. 7c), but with some ripple that distorts to some extent the waveform of phase currents (Fig. 7d). As a result, the control variables are properly regulated but the THD of phase currents increases up to 57.9%. Although FCS-MPC is known to provide some distortion in the x-y currents when a single switching state per sampling period is applied [36], the fact that instantaneous values are fully disregarded in the voltage selection also influences the final current quality. As it was explained in Section IV, this fact is especially remarkable in multistep FCS-MPC because the predictive algorithm tends to select switching states that cancel each other even when they have high (and opposite) values. This leads to the generation of virtual or quasi-virtual zeros in the x-y plane that generate a high amount of switching harmonics in this sensitive secondary plane. In fact, with this setting the zero-voltage vector is selected in k+3 only 56.13% of the time during the whole test, indicating that in some cases the FCS-MPC is considering active voltage vectors to mitigate secondary currents.

Aiming to jeopardize switching states with a high variability, increasing values of K_{sd} inform the predictive algorithm that couples of voltage vectors with a high standard deviation are not desirable. If the weighting factor K_{sd} is set to 1 and K_{xy} is nullified, then the predictive algorithm looks for low instantaneous values, but it does not care about averages values in the secondary subspace. Tests 1.2 evaluates this case, showing that the speed and currents are properly tracked, but the x-y and phase currents have a similar distortion as in Test 1.1. It is remarkable that with this setting of the weighting factors, the FCS-MPC algorithm always selects the zero vector as the optimum option in $k+3$ (cyan dots in Fig. 7e are null vectors, selected 100% of the time). This procedure ensures a low standard deviation, which is the last term in (7). Nevertheless, since the average values in the x-y plane are not considered, the algorithm only focuses on the elimination of the switching harmonics. Unfortunately, the appearance of non-null average x-y voltages also generates current harmonics that are mapped onto the secondary plane. For this reason, the final THD of phase currents is also elevated up to 54.98 %.

Finally, Test 1.3 shows the results for a setting when K_{xy}=0.5 and K_{sd}=0.75. Those weighting factors are tuned using a trial-and-error procedure to ensure a good tracking of the main variables and a low current distortion. Since both K_{xy} and K_{sd} are non-null, both the average and instantaneous values are considered now. In other words, the switching pattern is selected aiming to diminish both sources of current harmonics in the secondary plane, those related to non-null average x-y voltage, second term in (7), and those arising from the switching harmonics that are generated when high instantaneous voltages are applied within the sampling period, third term in (7). With this new setting, the tracking of the speed and d-q currents are similar to that in Tests 1.1 and 1.2, but the amount of x-y currents is highly decreased. This leads to a significant reduction of the phase current THD down to 36.18%, which is more than one third less than in previous Tests 1.1. and 1.2. The percentage of time for the null voltage vector in k+3 algorithm is now 97.75%, indicating that the third term in (7) is effectively avoiding the application of virtual zeros. At the same time, the second term in (7) influences the selection of the optimum switching state, and this results in a better current quality at this operating point.

For the sake of completeness, Test 2 evaluates the performance of the multistep FCS-MPC at a lower speed (200 rpm), considering the same settings used in Test 1, namely, null value of K_{sd} in Test 2.1, null value of K_{xy} in Test 2.2 and non-null values of both weighting factors in Test 2.3. The results are shown respectively, in the left, middle and right plots of Fig. 8. The speed and current tracking are again satisfactory in all cases, with no significant differences in the three settings under consideration. Nevertheless, the situation becomes different in the tracking of the secondary currents. Tests 2.1 and 2.2 have a similar x-y current ripple because each setting only diminishes one source of current harmonics: those related to non-null average x-y voltages are limited in Test 2.1, whereas switching harmonics due to a significant variation of x-y voltages within the considered sampling periods [10] are restricted in Test 2.2. The phase current THD in both cases is rather similar, but the origin of the ripple is of a different nature. As in Test 1, when K_{sd} is null the predictive strategy only selects a zero vector 66% of the time in k+3 in spite of the low-speed setting (and the associated low voltage requirements). This is so because the FCS-MPC is creating virtual zero (or quasi-zero) vectors with two active vectors in many cases, hence leading to higher switching harmonics. On the other hand, in Test 2.2 the zero vector is always selected in k+3 because it brings a low value of the standard deviation included in the third term of (7). This procedure limits the switching harmonics but at the same time does not care at all if the average x-y voltages are null or not, and this also provokes the appearance of current harmonics (in the form of the aforementioned second source). In the case of Test 2.3, both sources of current harmonics are simultaneously considered by the proposed multistep FCS-MPC thanks to the second and third terms of (7), respectively. Even though the predictive strategy needs to find a trade-off between both sources of current harmonics, the final result is a lower value of the x-y current ripple and a clear reduction (again more than 33% as it occurred in Test 1) of the phase current THD.

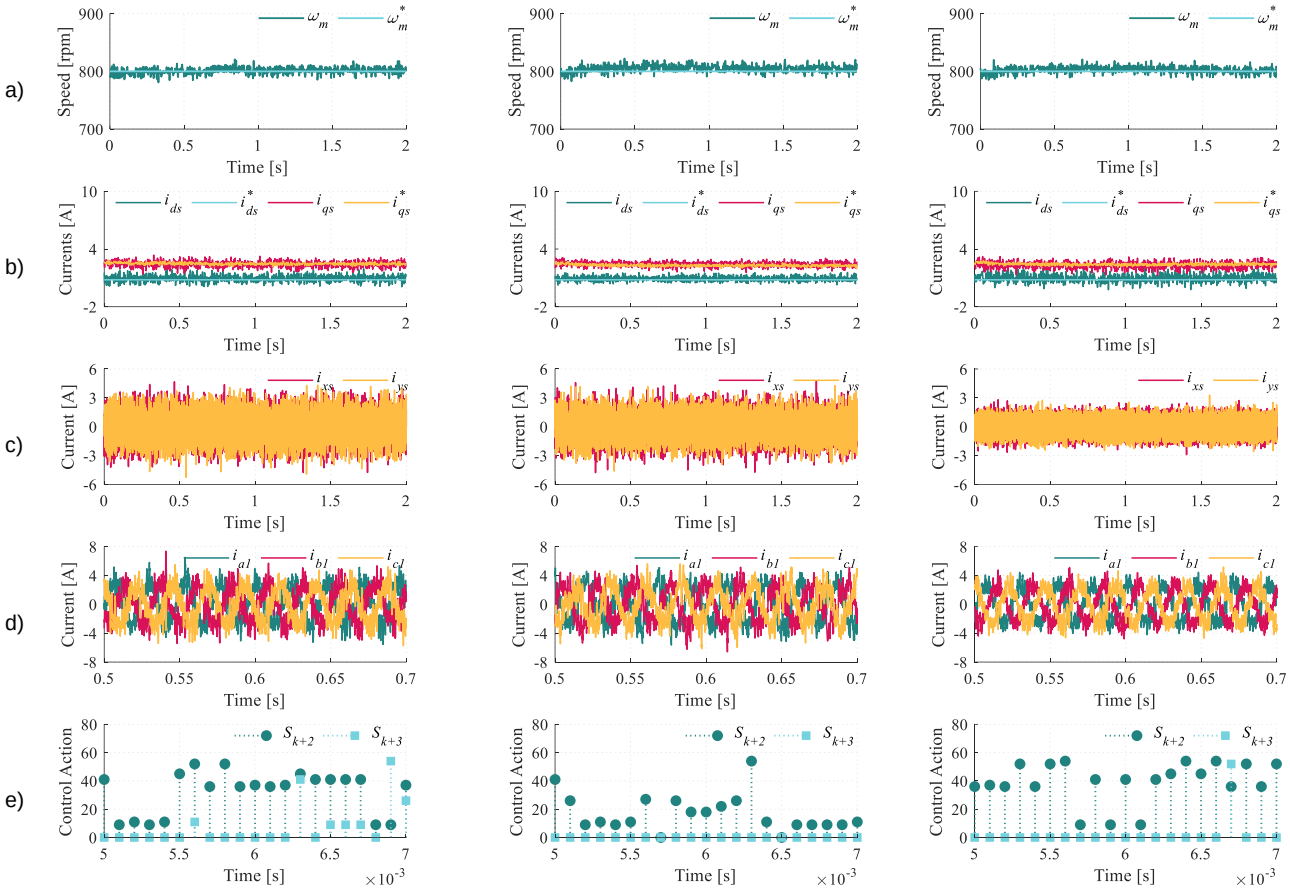

Fig. 7. Test 1: high current demand for FCS-MPC with K_{xy}=0.5 and K_{sd}=0 (left plots), FCS-MPC with K_{xy}=0 and K_{sd}=1 (middle plots) and FCS-MPC with K_{xy}=0.5 and K_{sd}=0.75 (right plots). From top to bottom: a) mechanical speed, b) d-q currents, c) x-y currents, d) set #1 of phase currents and e) zoom of the voltage vector selection. Corresponding switching frequencies: 2.00 kHz, 2.03 kHz and 1.72 kHz.

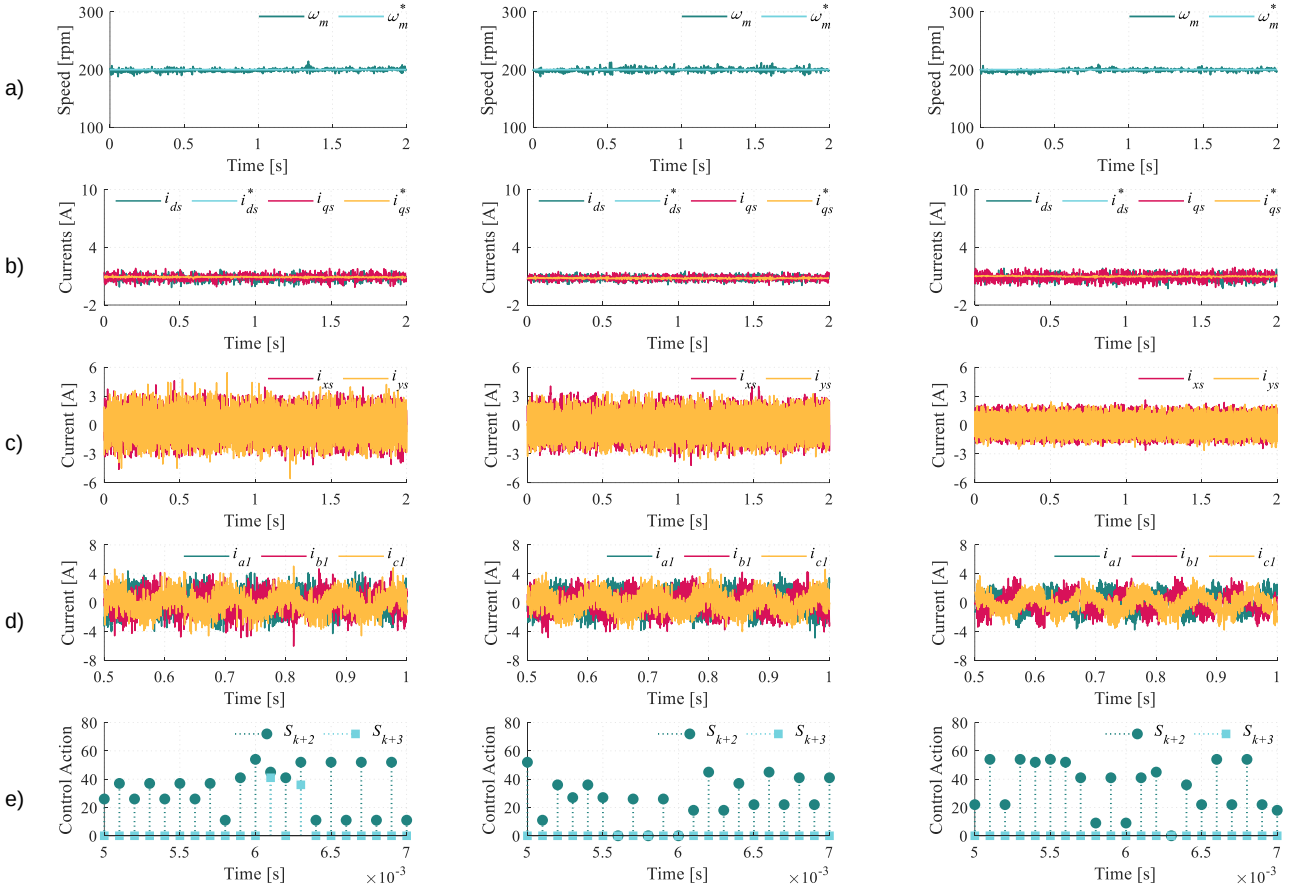

Fig. 8. Test 2: low current demand for FCS-MPC with K_{xy}=0.5 and K_{sd}=0 (left plots), FCS-MPC with K_{xy}=0 and K_{sd}=1 (middle plots) and FCS-MPC with K_{xy}=0.5 and K_{sd}=0.75 (right plots). From top to bottom: a) mechanical speed, b) d-q currents, c) x-y currents, d) set #1 of phase currents and e) zoom of the voltage vector selection. Corresponding switching frequencies: 3.17 kHz, 2.87 kHz and 1.97 kHz.

It follows that the current quality using the proposed multistep FCS-MPC is significantly higher than in the standard case that solely relies on averaged models.

Test 3 allows analysing the advantages of the proposed FCS-MPC scheme over the conventional FCS-MPC based on a single-step prediction horizon, where all the available voltage vectors have been defined as selectable control actions. This Test 3 is focused on a steady state situation with a high current demand as shown in Fig. 9. The left plots of Fig. 9 show the experimental results for the single-step strategy, whereas the performance of the proposed FCS-MPC has been depicted in the right plots. As shown in Fig. 9, both control techniques successfully track the d-q currents. However, if the mean squared error is calculated for the reference and measured q currents, the proposed method improves around 37% over the conventional FCS-MPC. Focusing on the secondary subspace (Fig. 9c), the multistep FCS-MPC also achieves a lower harmonic injection, thanks to the implemented smart voltage selection and the designed cost function. Consequently, the phase currents present a lower harmonic distortion than in the case of conventional FCS-MPC (see Fig. 9d). In fact, if the total harmonic distortion is calculated for the phase currents, the proposed FCS-MPC obtains a reduction of 22.22% in this quality index.

Concerning the dynamic response of the considered multistep FCS-MPC, Fig. 10 shows its performance when the reference speed is modified following a step profile (Test 4). Left plots of Fig. 10 are related to conventional FCS-MPC, whereas right plots are employed to illustrate the behavior of the proposed control scheme. The lower q-current error tracking of the developed multistep solution (Fig. 10b) permits obtaining a faster speed response as shown in Fig. 10a. Therefore, an additional advantage of the considered strategy is an enhanced dynamic response than in the case of FCS-MPC based on a single-step prediction horizon.

In the Test 5, the proposed FCS-MPC is compared with a multistep FCS-MPC where all the switching states are added as possible control actions in the different prediction steps. In both regulation techniques the control focus is defined in $k+3$. In this case, the proposed analysis has been carried out using numerical simulations due to the high computational cost of the multi-step MPC with all possible input combinations. The results of Test 5 have been depicted in Fig. 11, where the left plots show the performance of the proposed multistep FCS-MPC, and the right plots are related to the control solution described in this point. The addition of a higher number of voltage vectors permits the improvement of the main currents tracking (see Fig. 11). In fact, the d-q currents show a slightly higher ripple in the case of the proposed control scheme. Nevertheless, the situation is completely different if the secondary currents are analyzed (Fig. 11c). The control approach applied in the considered FCS-MPC permits reducing the x-y injection, because the selected control actions provide the better response in this subspace. Consequently, the phase currents are characterized by a lower harmonic distortion, as shown in Fig. 11d. Using the total harmonic distortion to illustrate the mentioned improvement, the proposal of the authors provides a reduction of 34.42% of this significant quality index. It is important to highlight that this enhancement of the current quality has been obtained with a significant reduction of computational burden, as shown in Table III.

Finally, the goodness of the proposed multi-step solution is tested considering the usage of several switching states per sampling period. In particular, the control actions designed in [20] (designed as VVs) and [31] (termed as LVVs) have been selected for that purpose. As previously exposed, the simple modification of Table I permits exploring these new control

TABLE III
COMPUTATIONAL BURDEN

Control method	Computational time (μs)
Single-step FCS-MPC	67
Proposed Multistep FCS-MPC	97
Multistep FCS-MPC using all available inputs	6871

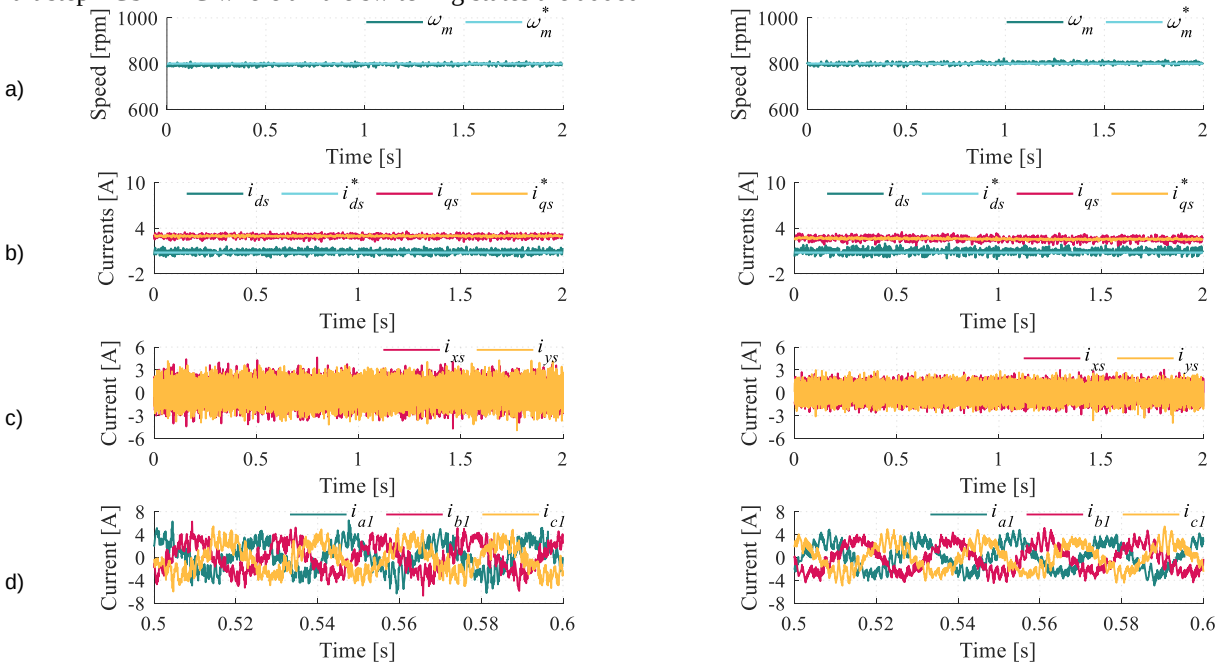

Fig. 9. Test 3: high current demand for standard FCS-MPC (left plots) and proposed multistep FCS-MPC with $K_{xy} = 0.2$ and $K_{sd} = 0.45$ (right plots). From top to bottom: a) mechanical speed, b) d-q currents, c) x-y currents and d) set #1 of phase currents. Corresponding switching frequencies: 1.66 kHz and 1.62 kHz.

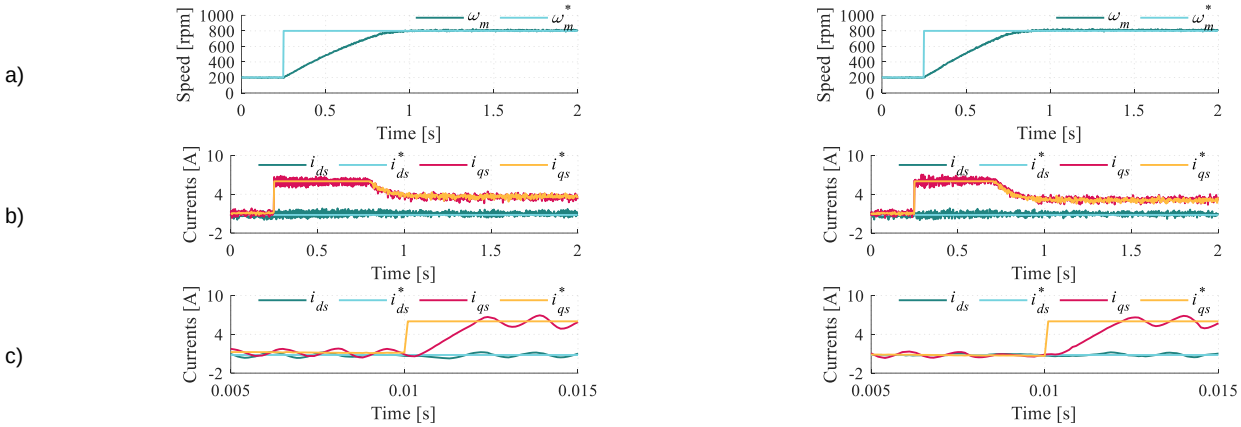

Fig. 10. Test 4: speed dynamic test for standard FCS-MPC (left plots) and proposed multistep FCS-MPC with $K_{xy} = 0.2$ and $K_{sd} = 0.45$ (right plots). From top to bottom: a) mechanical speed, b) d-q currents and c) zoom of the d-q currents.

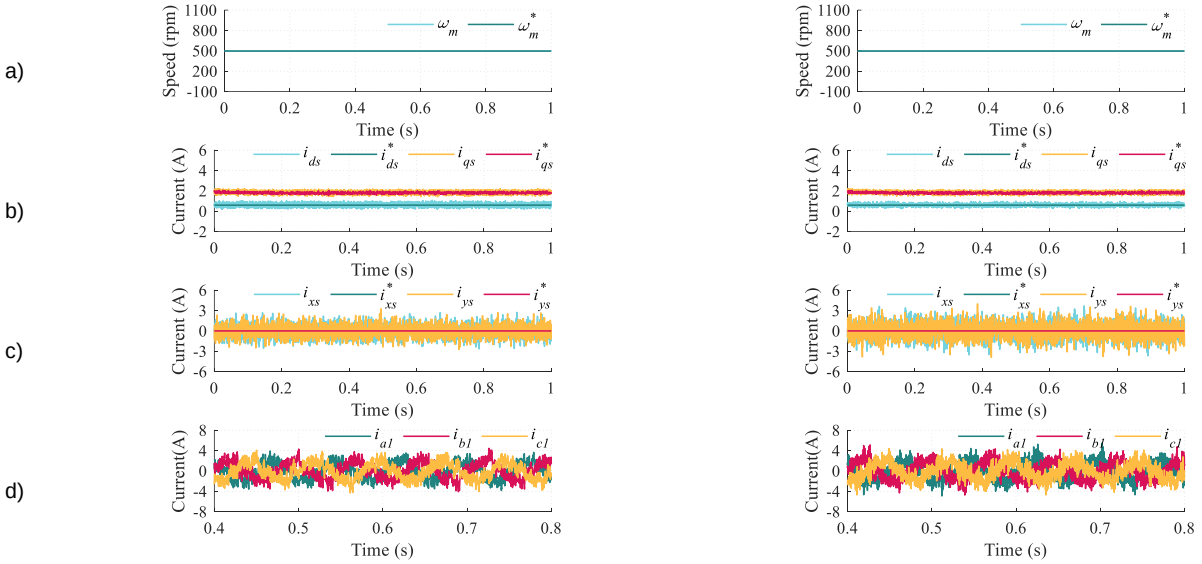

Fig. 11. Test 5: low current demand for the proposed multistep FCS-MPC (left plots) and a standard multi-step MPC with all possible input combinations (right plots). From top to bottom: a) mechanical speed, b) d-q currents, c) x-y currents and d) set #1 of phase currents. Corresponding switching frequencies: 1.16 kHz and 1.17 kHz.

scenarios. In fact, in this Test 6 three different sets of control actions have been implemented. Fig. 12 shows the diagrams of α-β and x-y currents for the considered control actions when a single (left plots) and a multi-step (right plots) prediction horizon are implemented. This Fig. 12. can be analyzed per rows and columns. As expected, the inclusion of multi-vector control actions permits reducing the secondary components. In fact, this trend can be observed regardless of the employed prediction horizon (see rows of Fig. 12). Focusing on the study by columns, the reader can see the benefits of the implementation of a multi-step scheme. For instance, regardless of the implemented set of control actions, the proposed control solution provides a better regulation of the main components.

V. Conclusions

While FCS-MPC with a one-step prediction horizon can be implemented for six-phase electric drives evaluating all switching states (64 when supplied from two-level VSCs), such an exhaustive search cannot be implemented in real-time if multistep predictive control is used. Fortunately, it is possible to highly reduce the search possibilities if physical considerations are taken into account. Medium-large, medium, and small voltage vectors prove to be inappropriate

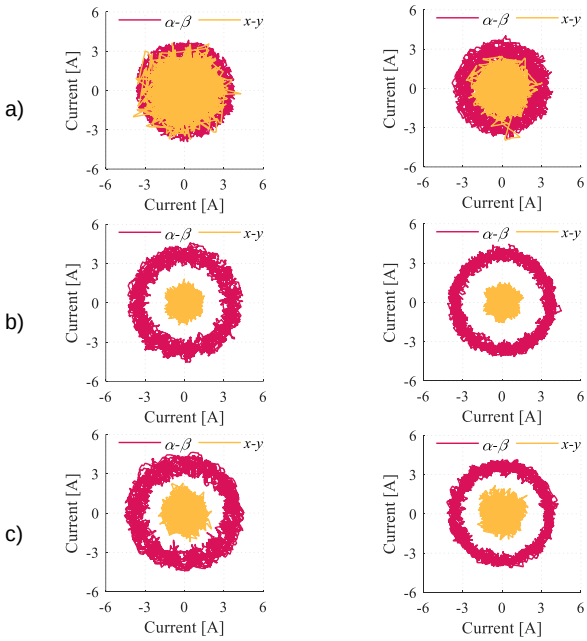

Fig. 12. Diagrams of α-β and x-y currents for control schemes with a single-step prediction horizon (left plots) and control schemes based on a multi-step prediction horizon (right plots). From top to bottom: a) a single switching state per control period, b) VVs as control actions and c) LVVs as active voltage outputs.

in distributed-winding multiphase machines with a low x-y impedance, hence only large and zero vectors should be considered in the initial step. Then, the voltage vectors for the second step can be restricted by considering that the α-β voltage vector describes a circle in steady state. This simplification reduces the number of iterations from 4096 to 52. Experimental results confirm that the real-time implementation of the proposed multistep FCS-MPC is feasible.

Nevertheless, initial implementations showed that the two-step approach tended to skip the selection of zero vectors in favor of active vectors in phase opposition. The predictive algorithm was *deceived* by the sole consideration of the average values. Fortunately, a rather simple modification can inform the FCS-MPC that such a procedure is inappropriate. The inclusion of a term related to the standard deviation within the newly proposed cost function promotes the use of true zero vectors at the expense of the creation of virtual zeros. This sole modification improves the THD of phase currents by 37%, hence improving the current quality and reducing the stator copper losses.

In addition, thanks to the proposed control structure, the advantages of the developed multi-step algorithm can also be exploited when several switching states are applied per control period. In fact, two well-known multi-vector solutions have been explored with the considered multi-step scheme obtaining an additional improvement in the control performance.

REFERENCES

[1] H. A. Toliyat, T. A. Lipo and J. C. White, "Analysis of a concentrated winding induction machine for adjustable speed drive applications. I. Motor analysis," *IEEE Trans. Energy Conv.*, vol. 6, no. 4, pp. 679-683, Dec. 1991.

[2] H. A. Toliyat, T. A. Lipo and J. C. White, "Analysis of a concentrated winding induction machine for adjustable speed drive applications. II. Motor design and performance," *IEEE Trans. Energy Conv.*, vol. 6, no. 4, pp. 684-692, Dec. 1991.

[3] E. Levi, M. Jones, S. N. Vukosavic and H. A. Toliyat, "A novel concept of a multiphase, multimotor vector controlled drive system supplied from a single voltage source inverter," *IEEE Trans. Power Electron.*, vol. 19, no. 2, pp. 320-335, March 2004.

[4] E. Jung, H. Yoo, S. Sul, H. Choi and Y. Choi, "A Nine-Phase Permanent-Magnet Motor Drive System for an Ultrahigh-Speed Elevator," *IEEE Trans. Ind. Appl.*, vol. 48, no. 3, pp. 987-995, May-June 2012.

[5] Mercerdes-AMG EQE 53 4MATIC+, https://www.mercedes-amg.com/en/world-of-amg/news/press-information/mercedes-amg-eqs-53.html online available, accessed August 2022.

[6] Audi e-tron FE07, https://www.audi-mediacenter.com/en/press-releases/audi-presents-e-tron-fe07-for-formula-e-world-championship-13365 online available, accessed August 2022.

[7] E. Levi, "Multiphase Electric Machines for Variable-Speed Applications," *IEEE Trans. Ind. Electron.*, vol. 55, no. 5, pp. 1893-1909, 2008.

[8] E. Levi, R. Bojoi, F. Profumo, H. Toliyat, S. Williamson, "Multiphase Induction Motor Drives-A Technology Status Review," *IET Electr. Power Appl.*, vol. 1, no. 4, pp. 489-516, 2007.

[9] F. Barrero, M. R. Arahal, R. Gregor, S. Toral and M. J. Duran, "A Proof of Concept Study of Predictive Current Control for VSI-Driven Asymmetrical Dual Three-Phase AC Machines," *IEEE Trans. Ind. Electron.*, vol. 56, no. 6, pp. 1937-1954, June 2009.

[10] M. Duran, I. Gonzalez-Prieto, A. Gonzalez-Prieto and J. J. Aciego, "The Evolution of Model Predictive Control in Multiphase Electric Drives: A Growing Field of Research," *IEEE Ind. Electron. Mag*. doi: 10.1109/MIE.2022.3169291.

[11] M. J. Duran, J. Prieto, F. Barrero and S. Toral, "Predictive Current Control of Dual Three-Phase Drives Using Restrained Search Techniques," *IEEE Trans. Ind. Electron.*, vol. 58, no. 8, pp. 3253-3263, Aug. 2011.

[12] I. González-Prieto, I. Zoric, M. J. Duran and E. Levi, "Constrained Model Predictive Control in Nine-Phase Induction Motor Drives," *IEEE Trans. Energy Conv.*, vol. 34, no. 4, pp. 1881-1889, Dec. 2019.

[13] C. Martín, M. R. Arahal, F. Barrero and M. J. Durán, "Five-Phase Induction Motor Rotor Current Observer for Finite Control Set Model Predictive Control of Stator Current," *IEEE Trans. Ind. Electron.*, vol. 63, no. 7, pp. 4527-4538, July 2016.

[14] A. Tani, M. Mengoni, L. Zarri, G. Serra and D. Casadei, "Control of Multiphase Induction Motors With an Odd Number of Phases Under Open-Circuit Phase Faults," *IEEE Trans. Power Electron.*, vol. 27, no. 2, pp. 565-577, Feb. 2012.

[15] S. Dwari and L. Parsa, "An Optimal Control Technique for Multiphase PM Machines Under Open-Circuit Faults," *IEEE Trans. Ind. Electron.*, vol. 55, no. 5, pp. 1988-1995, May 2008.

[16] C. Martin, M. Bermudez, F. Barrero, M. R. Arahal, X. Kestelyn and M. J. Duran, "Sensitivity of predictive controllers to parameter variation in five-phase induction motor drives", *Control Eng. Pract.*, vol. 68, pp. 23-31, Nov. 2017.

[17] M. R. Arahal, F. Barrero, M. J. Duran, M. G. Ortega and C. Martin, "Trade-offs analysis in predictive current control of multi-phase induction machines", *Control Eng. Pract.*, vol. 81, pp. 105-113, Dec. 2018.

[18] M. J. Duran, I. Gonzalez-Prieto, F. Barrero, E. Levi, L. Zarri and M. Mengoni, "A Simple Braking Method for Six-Phase Induction Motor Drives With Unidirectional Power Flow in the Base-Speed Region," *IEEE Trans. Ind. Electron.*, vol. 64, no. 8, pp. 6032-6041, Aug. 2017.

[19] I. Subotic, N. Bodo, E. Levi and M. Jones, "Onboard Integrated Battery Charger for EVs Using an Asymmetrical Nine-Phase Machine," *IEEE Trans. Ind. Electron.*, vol. 62, no. 5, pp. 3285-3295, May 2015.

[20] I. González-Prieto, M. J. Durán, M. Bermúdez, F. Barrero and C. Martín, "Assessment of Virtual-Voltage-Based Model Predictive Controllers in Six-Phase Drives Under Open-Phase Faults," *IEEE Trans. Emerg. Sel.*, vol. 8, no. 3, pp. 2634-2644, Sept. 2020.

[21] A. González-Prieto, I. González-Prieto, M. J. Duran, J. J. Aciego and P. Salas-Biedma, "Current Harmonic Mitigation Using a Multi-Vector Solution for MPC in Six-Phase Electric Drives," *IEEE Access*, vol. 9, pp. 117761-117771, 2021.

[22] H. Wang, X. Wu, X. Zheng and X. Yuan, "Virtual Voltage Vector Based Model Predictive Control for a Nine-Phase Open-End Winding PMSM With a Common DC Bus," *IEEE Trans. Ind. Electron.*, vol. 69, no. 6, pp. 5386-5397, June 2022.

[23] A. Bhowate, M. V. Aware and S. Sharma, "Speed Sensor-Less Predictive Torque Control for Five-Phase Induction Motor Drive Using Synthetic Voltage Vectors," *IEEE Trans. Emerg. Sel.*, vol. 9, no. 3, pp. 2698-2709, June 2021.

[24] C. Xiong, H. Xu, T. Guan, and P. Zhou, "A constant switching frequency multiple-vector-based model predictive current control of five-phase PMSM with nonsinusoidal back EMF," *IEEE Trans. Ind. Electron.*, vol. 67, no. 3, pp. 1695–1707, Mar. 2020.

[25] M. Ayala, J. Doval-Gandoy, J. Rodas, O. Gonzalez, R. Gregor and M. Rivera, "A Novel Modulated Model Predictive Control Applied to Six-Phase Induction Motor Drives," *IEEE Trans. Ind. Electron.*, vol. 68, no. 5, pp. 3672-3682, May 2021.

[26] P. Karamanakos et al. "Model Predictive Control of Power Electronic Systems: Methods, Results, and Challenges." *IEEE Open Journal of Industry Applications*, no. 1, pp. 95–114, Sept. 2020.

[27] J. Rodriguez et al., "Latest Advances of Model Predictive Control in Electrical Drives—Part II: Applications and Benchmarking With Classical Control Methods," *IEEE Trans. Power Electron.*, vol. 37, no. 5, pp. 5047-5061, May 2022.

[28] T. Geyer and D. E. Quevedo, "Performance of Multistep Finite Control Set Model Predictive Control for Power Electronics," *IEEE Trans. Power Electron.*, vol. 30, no. 3, pp. 1633-1644, March 2015.

[29] P. Karamanakos, T. Geyer, N. Oikonomou, F. D. Kieferndorf and S. Manias, "Direct Model Predictive Control: A Review of Strategies That Achieve Long Prediction Intervals for Power Electronics," *IEEE Ind. Electron. Mag.*, vol. 8, no. 1, pp. 32-43, March 2014,

[30] X. Li, Q. Yang, W. Tian, P. Karamanakos and R. Kennel, "A Dual Reference Frame Multistep Direct Model Predictive Current Control With a Disturbance Observer for SPMSM Drives," *IEEE Trans. Power Electron.*, vol. 37, no. 3, pp. 2857-2869, March 2022.

[31] H. Xie, L. Liu, Y. He, F. Wang, J. Rodríguez and R. Kennel, "Gradient Descent-Based Objective Function Reformulation for Finite Control Set Model Predictive Current Control With Extended Horizon," *IEEE Trans. Ind. Electron.*, vol. 69, no. 9, pp. 8667-8678, Sept. 2022.

[32] M. Abu-Ali, F. Berkel, M. Manderla, S. Reimann, R. Kennel and M. Abdelrahem, "Deep Learning-Based Long-Horizon MPC: Robust, High Performing, and Computationally Efficient Control for PMSM Drives," *IEEE Trans. Power Electron.*, vol. 37, no. 10, pp. 12486-12501, Oct. 2022.

[33] T. Dorfling, H. du Toit Mouton, T. Geyer and P. Karamanakos, "Long-Horizon Finite-Control-Set Model Predictive Control With

Nonrecursive Sphere Decoding on an FPGA," *IEEE Trans. Power Electron.*, vol. 35, no. 7, pp. 7520-7531, July 2020

[34] M. J. Duran, E. Levi, and F. Barrero, "*Multiphase electric drives: Introduction*," Wiley Ency. Electr. and Electron. Engr., pp. 1-26, 2017.

[35] M. J. Durán, J. Prieto, F. Barrero, J. A. Riveros and H. Guzman, "Space-Vector PWM With Reduced Common-Mode Voltage for Five-Phase Induction Motor Drives," *IEEE Trans. Ind. Electron., vol. 60, no. 10, pp. 4159-4168, Oct. 2013.*

[36] M. J. Durán, I. Gonzalez-Prieto, and A. Gonzalez-Prieto, "Large virtual voltage vectors for direct controllers in six-phase electric drives," *Int. J. Electr. Power Energy Syst.*, vol. 125, 2021.

[37] H. S. Che, E. Levi, M. Jones, W. -P. Hew and N. A. Rahim, "Current Control Methods for an Asymmetrical Six-Phase Induction Motor Drive," *IEEE Trans. Power Electron*., vol. 29, no. 1, pp. 407-417, Jan. 2014.

[38] Y. Zhao and T. A. Lipo, "Space vector PWM control of dual three-phase induction machine using vector space decomposition," *IEEE Trans. Ind. Appl.*, vol. 31, no. 5, pp. 1100-1109, Sept.-Oct. 1995.

[39] A. G. Yepes *et al.*, "Parameter identification of multiphase induction machines with distributed windings—Part 1: Sinusoidal excitation methods," *IEEE Trans. Energy Convers.*, vol. 27, no. 4, pp. 1056 1066, Dec. 2012.

[40] J. A. Riveros *et al.*, "Parameter identification of multiphase induction machines with distributed windings—Part 2: Time-domain techniques," *IEEE Trans. Energy Convers.*, vol. 27, no. 4, pp. 1067–1077, Dec. 2012.

Ignacio González-Prieto was born in Malaga, Spain, in 1987. He received the Industrial Engineer and M.Sc. degrees in Fluid Mechanics from the University of Malaga, Malaga, Spain, in 2012 and 2013, respectively, and the Ph.D. degree in electronic engineering from the University of Seville, Sevilla, Spain, in 2016. His research interests include multiphase electric drives, wind energy systems, and electrical vehicles.

Mario J. Duran was born in Bilbao, Spain, in 1975. He received the M.Sc. and Ph.D. degrees in electrical engineering from the University of Malaga, Malaga, in 1999 and 2003, respectively. He is currently a Full Professor in the Department of Electrical Engineering, University of Malaga. His research interests include modeling and control of multiphase drives and renewable energies conversion systems.

Angel Gonzalez-Prieto was born in Malaga, Spain, in 1993. He received the University and M. Sc. degrees in Industrial Engineering from the University of Malaga, Malaga, Spain, in 2017 and 2019, respectively. He is currently developing his Ph.D. in Electric Energy Systems Program at the University of Malaga. His research interests include multiphase machines and renewable energy conversion system.

Juan Jose Aciego was born in Malaga, Spain, in 1976.He received the Industrial Engineer and M.Sc. degrees from the University of Malaga, Malaga, Spain, in 2010 and 2016, respectively and the Ph.D. degree in Electric Systems the University of Malaga, Malaga, Spain, in 2022.
His research interests include power modeling and control of multiphase drives, renewable energy conversion systems and electric vehicles.